Additive manufacturing and characterization of microstructures using two-photon polymerization for use in cryogenic applications

Sherman E. Peek[1,2,3,a] , **Jacob Ward**[1,2], **Stephen Bankson**[1,2], **Archit Shah**[1,2] ,
John A. Sellers[1,2] , **Mark L. Adams**[1,2,3] , **Michael C. Hamilton**[1,2]

[1] *Department of Electrical and Computer Engineering, Auburn University, Auburn, AL, USA*
[2] *Alabama Micro/Nano Science and Technology Center (AMNSTC), Auburn University, Auburn, AL, USA*
[3] *Systems Visions LLC, Auburn, AL, USA*
[a] Address all correspondence to this author. e-mail: sep0022@auburn.edu

Fabricating polymer structures for use at cryogenic temperatures is a non-trivial task due to coefficient of thermal expansion mismatches and stresses that are induced because of this mismatch. This work demonstrates a viable process to additively fabricate polymer microstructures using two-photon polymerization (TPP) on silicon substrates with tetraethylorthosilicate oxide for use at cryogenic temperatures. The process of creating the polymerized structures using resins SR368 and SR499, as well as its application onto the target substrate is detailed. The importance of pre-fabrication adhesion layer processing is discussed and post-polymerization procedures are described. Cryogenic thermal cycling was performed by direct submersion into liquid nitrogen to assess worst-case degradation due to thermal shock and exhibited encouraging shear load failure performance after thermal cycling. The reliability of the test structures demonstrated in this work shows promise for implementing more complex structures using TPP for use at cryogenic temperatures.

Introduction

Additive manufacturing is an ever-expanding field within materials research. From simple prototyping to production, additive manufacturing has become a cost-effective and widespread method of developing products. From laser direct writing approaches to aerosol material jetting techniques, work is continuing to increase material compatibility, as well as increasing printed resolution and uniformity. Challenges with additive manufacturing are the overall resolution, accuracy, and repeatability of the processes since many processes are highly dependent on environmental factors [1, 2]. Additionally for additive manufacturing to be particularly useful for micro/nano-scale applications, material compatibility and resolution are of utmost importance. Two-photon polymerization (TPP, otherwise known as multi-photon polymerization) is a potential solution to these challenges. TPP differs from standard selective light processes in that polymerization occurs within a smaller volume in the interior of the focal

volume, also known as a voxel [3]. In selective light manufacturing, control of the power directly influences manufacturing such that, above a polymerization threshold, polymerization occurs. The mechanics behind TPP are fundamentally identical, however an additional mechanism is leveraged to reduce the polymerization volume, reduce necessary power to achieve polymerization, and increase resolution by reducing the size of the voxel. If an ultra-short pulse and high repetition rate laser is used to irradiate a photo-definable sample (i.e., materials that chemically react and cross-link with a photoinitiator), energy of photons combine to elevate the effective energy in a particular location (usually within the focal volume as previously described) since the energy decay rate is lower than the introduction rate of a second photon. This mechanism has been commonly referred to as two-photon absorption [4]. The rate of combination is significantly higher nearer the center of a Gaussian laser due to the photon density (or photon flux) distribution of the beam. The significance of polymerization that is facilitated by two-photon absorption is that it can allow

for feature sizes below the diffraction limit [5], a unique trait belonging to this additive manufacturing method.

Example applications that use TPP for additive manufacturing are mechanical structures such as cantilevers [6] and photonic connectors [7]. For each of these applications, common parameters that affect the fabrication quality are wavelength (photon energy), pulse duration, scanning speed, numerical aperture, and resin composition (viscosity and photo-polymerization sensitivity) [8]. Depending on degree of polymerization and material composition, it was found that optical and structural properties can be altered for a tuned performance [9].

Though TPP is an intriguing option for fabricating structures with micro- and nano-scale feature sizes, many challenges are present with the technique and many factors affect the outcome and flexibility of the process. TPP by nature is a serial process much like many other selective light processes. Scaling this technology for mass production is challenging and costly since the most available solution is to implement a parallel approach by splitting a high power laser and using multiple optical fabrication setups. In addition, material compatibility is not well explored for TPP largely due to the required specialized equipment being a significant barrier to entry to begin experimentation and due to the numerous material combinations available [10, 11]. Commercial systems are available with formulated resin mixtures to alleviate challenges of custom chemistry to achieve a more turnkey end-user tool [12], however the range of resin options for these systems is lacking for more specific applications. Additionally, TPP-fabricated structures have been commonly used for room temperature applications but with the increasing interest in cryogenic and quantum applications, material and process verification is desirable to identify TPP as a viable process for low temperature usage. Integration with existing micro and nano fabrication materials and processes is paramount for expanding and integrating the usage of TPP with present cryogenic electronic and photonic technologies.

This work seeks to demonstrate that TPP is a viable option for microfabricated structures for use at cryogenic temperatures (e.g., as low as 77 K) by evaluating the structural stability of the fabricated structures and adhesion to SiOx before and after wide-temperature range, cryogenic thermal cycling. The largest concern of microstructures at cryogenic temperatures are stresses that are induced during large temperature changes from coefficient of thermal expansion mismatches. One common failure mode due to these stresses is delamination of the polymer structures from substrates [13]. This work describes fabrication processes and testing methodologies that target the structural integrity and adhesion failure mode of TPP-fabricated microstructures before and after cryogenic thermal cycling using a previously published resin formulation [14]. Evaluation of the fabrication processes used is detailed in the next section. The fabrication processes used to realize TPP microstructures are described in detail in the "Materials and Methods" section.

Results and discussion

This section begins with an evaluation of the fabricated structures after which further mechanical characterizations are detailed. Characterizations of TPP-fabricated microstructures were carried out to evaluate structural print quality as well as mechanical performance pre- and post-cryogenic thermal cycling.

Test structures

Structures fabricated in this work varied by sample preparation procedure and laser exposure dose. Test structures generally consisted of SR368 and SR499 acrylic monomers. A first solution that this work sought to find was an adhesion process to SiOx. From initial experiments without the use of a proper adhesion promotion procedure, TPP structure adhesion to SiOx was observed to be insufficient and yielded structures unable to quantifiably evaluate, as shown in Fig. 1, where excess resin rinsing after structure fabrication caused delamination of structures directly rinsed and the presumed beginning of delamination in the corners of structures indirectly rinsed. After a sufficient adhesion promotion process was developed (the use of methacryloxypropytrimethoxysilane, MPTS, in a silanization procedure, further detailed in "Materials and Methods" section), scanning electron microscopy (SEM) of a representative 400 × 400 μm TPP microstructure (sputtered with Au for visualization aid after excess resin was removed by solvent spray rinsing) was captured and is shown in Fig. 2. Though structures fabricated appear largely uniform, rounding of a singular side of structures was observed and is presumed due to resin movement and pileup during laser exposure process. Additionally, including
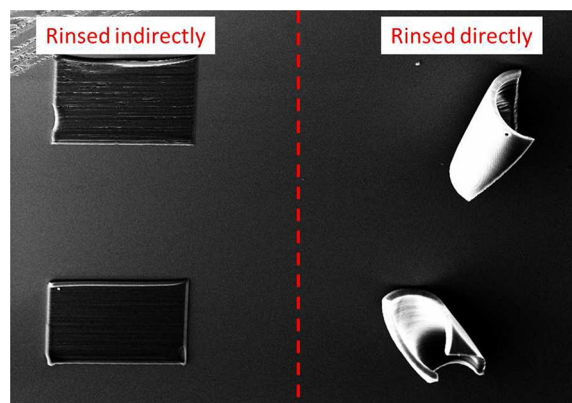

Figure 1: SEM image of TPP-fabricated microstructures (400 × 400 μm, 72× magnification) without an adhesion promotion layer. Delamination at SiOx interface occurred immediately during excess resin rinsing step.
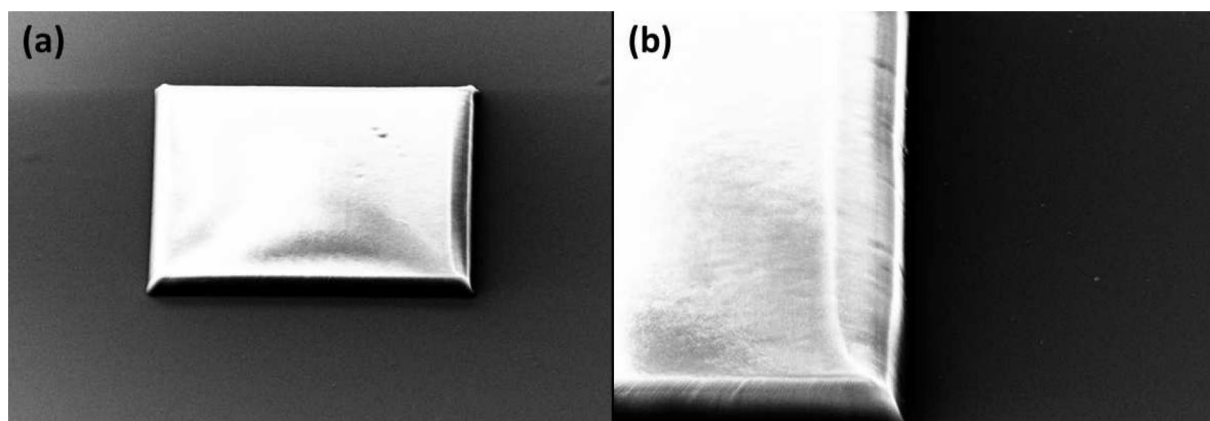
Figure 2: (a) SEM image of a representative TPP-fabricated test structures (400 × 400 µm, 154× magnification) and (b) zoom image (468x magnification) of a singular side wall capture that was observed to be rounded due to resin shift during TPP writing.

the adhesion procedure was observed to have minimal impact on the excess resin solvent rinsing in that the Si surface was observed to be clean after the rinsing procedure.

Materials properties

Atomic force microscopy (AFM) was used to capture surface roughness and force-distance measurements of representative microstructures. Results are shown in Fig. 3 demonstrating sufficient surface flatness of ± 400 nm that can be improved by using a higher numerical aperture objective to increase TPP print resolution as well as by improving the design fill parameters. Based on the surface roughness measurements, locations for force-distance measurements were selected based on peaks and valleys in the TPP-fabricated surface to evaluate the elastic modulus (E), results demonstrated in Table 1. Based on previous work from [9], variation in elastic modulus observed in collected measurements indicate nonuniformity in the degree of polymerization across sections of the fabricated structure. This further supports an observed trend where the valleys yielded lower elastic modulus and the peaks yielded higher elastic modulus, assuming that the surface height variation is caused by polymerization variation. Even when considering the minimum structure height fabricated in this work was greater than 5 µm, a worst case ± 8% surface variation relative to structure height is sufficient to evaluate the failure mode for cryogenic temperatures. Furthermore, with this level of polymerization and property variation, these structures survived and retained mechanical stability through cryogenic exposure, as discussed in the next section.

Failure mode evaluation

A single fabricated layer was desirable for adhesion evaluation by way of shear testing to eliminate additional failure modes such as printed layer delamination. The failure mode was first identified by shear testing structures with varying heights. Heights of the fabricated structures were controlled by adjusting the sample's (z-axis) position within the focal volume of the laser. The adhesion failure mode was verified experimentally by comparing shear load failure forces across multiple test structure heights before and after cryogenic thermal cycling for two cases of average laser source power (1 mW and 0.5 mW). Since the cross section of the adhesion interface (x,y) when evaluating adhesion in the presence of a shear stress is independent to the height of the structure [15], minimal correlation was expected if test structure to substrate interface adhesion is the primary failure mode. A diagram of the load shear testing relative to a microfabricated TPP test structure is demonstrated in Fig. 4. As shown in Fig. 5, no significant trends were identified when comparing the load shear failure force versus structure height, especially for the 0.5 mW case. Data were analyzed by extracting Kendall correlations for each set of data with coefficients being 0.74, – 0.30, 0.43, and 0.33 for each of the parameter sets (1 mW at room temperature, 1 mW after thermal cycling, 0.5 mW at room temperature, and 0.5 mW after thermal cycling), respectively. Kendall correlation method was selected over Pearson correlation method due to failed method criteria (regular interval) that would qualify the data for the Pearson correlation method. Additionally, Kendall correlations are a more robust metric for limited sample sizes. Since extracted coefficients were relatively low (except for the 1 mW at room temperature case) and varied when compared to themselves, the analysis lends to adhesion being the most probable primary failure mode. To confirm that the lower structure height failures were not due to the physical dimensions, an analysis of each fabricated chip was conducted. Fig. 6 shows the failure analysis organized by fabricated chips suggesting that fabrication variation was the cause of early failure in select structures, as apparent by the collection
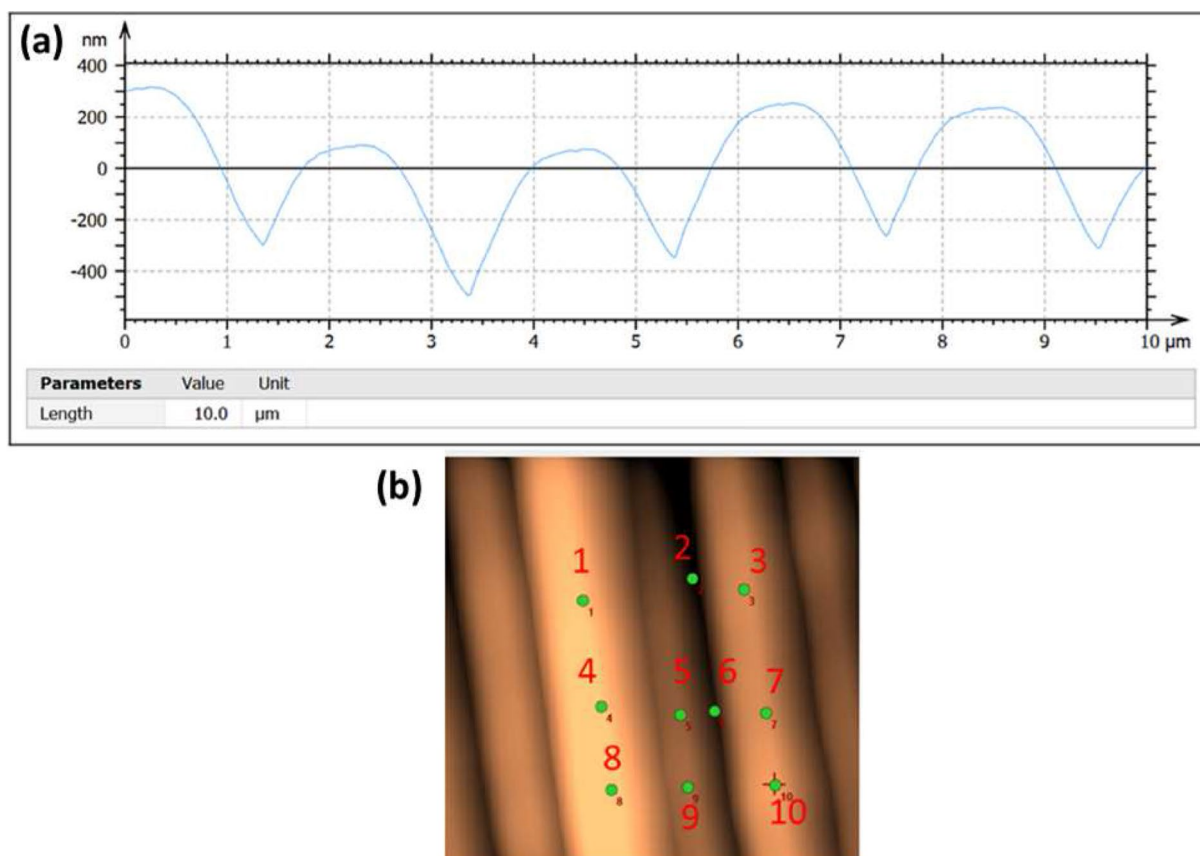
Figure 3: (a) AFM surface roughness measurement demonstrating ± 400 nm surface roughness. (b) Locations probed (denoted by red text and green dots) with AFM force-distance measurements to extract the local elastic modulus. Locations were selected based on extremes in surface roughness.

TABLE 1: Table of elastic modulus values extracted from locations defined in Fig. 3.

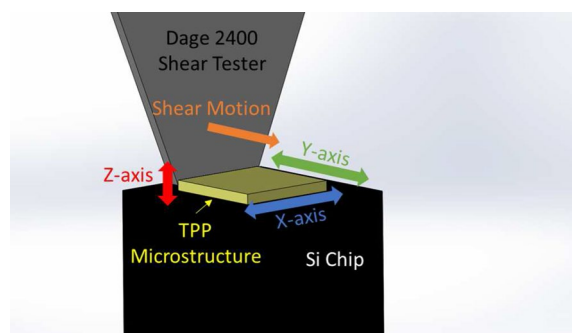| Location	E (GPa)	Location	E (GPa)
1	2.84	6	0.61
2	1.81	7	4.44
3	7.11	8	3.14
4	2.57	9	5.80
5	2.40	10	6.09

Figure 4: Schematic representation of the shear testing process, not to scale. The TPP microstructure is visualized in yellow, the Si chip is visualized in black, and the shear testing tool is visualized in grey.

of low shear load failures on particular chips. From the data collected, minimal thermal cycling degradation was observed and was determined to be most affected by fabrication variation rather than heights of structures.

Failure analysis

Experiments performed validated the failure mode to be the adhesion interface of the TPP microstructure to SiOx when using MPTS as the adhesion layer for structure heights less than 120 μm. With this information collected, the average load to failure shear stress for each of the four cases (0.5 mW average source power without cryogenic thermal cycling, 0.5 mW average source power after cryogenic thermal cycling, 1.0 mW
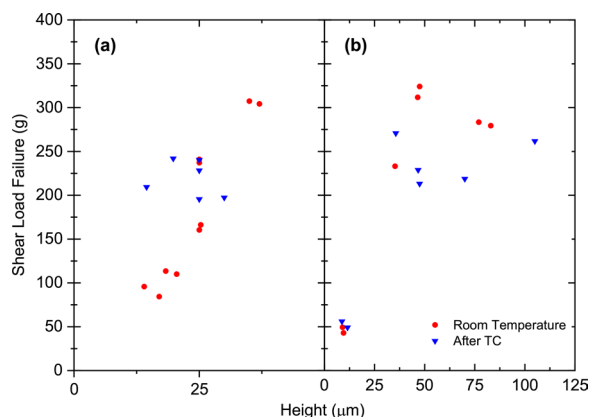
Figure 5: Shear load failure force versus structure height of test structures fabricated using (a) 1.0 mW and (b) 0.5 mW average laser source power tested before thermal cycling (room temperature) and after thermal cycling (TC). Data were analyzed by extracting Kendall correlations for each set of data with coefficients being 0.74, − 0.30, 0.43, and 0.33 for each of the parameter sets (1 mW at room temperature, 1 mW after thermal cycling, 0.5 mW at room temperature, and 0.5 mW after thermal cycling), respectively.
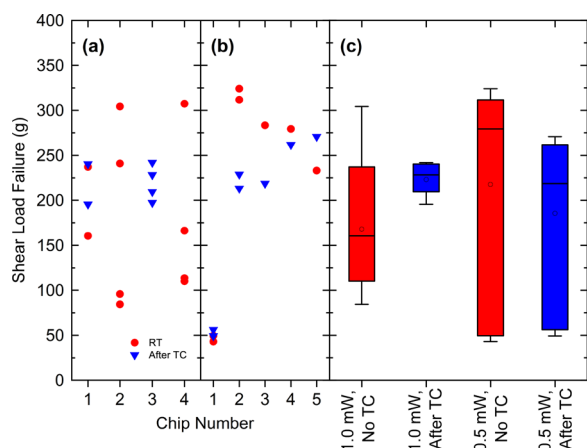

Figure 6: Figures evaluating (a) shear load failure force versus fabricated chips of structures fabricated with 1.0 mW average power before thermal cycling (room temperature, RT) and after thermal cycling (TC), (b) shear load failure force versus fabricated chips of structures fabricated with 0.5 mW average power before thermal cycling (room temperature, RT) and after thermal cycling (TC), and (c) condensing results into four major criteria.

average source power without cryogenic thermal cycling, and 1.0 mW average source power after cryogenic thermal cycling) was calculated by:

$$S = \frac{mg}{A}, \tag{1}$$

where S is the shear strength in Pa, m is the force measured in kg, g is acceleration (assumed 10 m/s^2), A is the in-plane surface area in m^2. Results were found to be 13.3 MPa, 11.4 MPa, 11.1 MPa, and 13.4 MPa, respectively. Significant fabrication

variation was observed to be the primary factor in determining the failure magnitude which strongly influences performed calculations. Yield of characterized structures was calculated and is presented in Fig. 7. For determining the yield of fabricated structures, a shear force of 150 g was selected as the minimum threshold from previous experiences using acrylic polymers at cryogenic temperatures [16]. Using this criteria, premature failure was observed with 6 of 17 measured structures failing at room temperature without any cryogenic temperature exposure. Additionally, promise in cryogenic viability was demonstrated by only 2 of 13 being observed as defective after cryogenic thermal cycling. Though yield should see improvement before scaling is viable, a greater than 70% total yield was encouraging in the context of this work where further process improvements are expected to improve the overall yield. Even through existing fabrication variation, the fabrication processes developed appear to be viable mechancially for cryogenic applications and the testing methodology used was observed to be sufficient for evaluating the mechanical reliability of the structures, including the adhesion to SiOx after a developed silanization process was implemented. Results presented give reason to continue TPP fabrication exploration and refinement for cryogenic applications.

Conclusion

This work meets the challenge of using additive manufacturing for cryogenic applications with a viable fabrication process and testing methodology. Initial efforts presented in this work described and solved issues of TPP structure adhesion to SiOx with a commercially available adhesion promoter, commonly used with acrylic polymers such as SU-8. Structural analysis was performed on TPP-fabricated microstructures (using a previously published resin formulation) with scanning electron
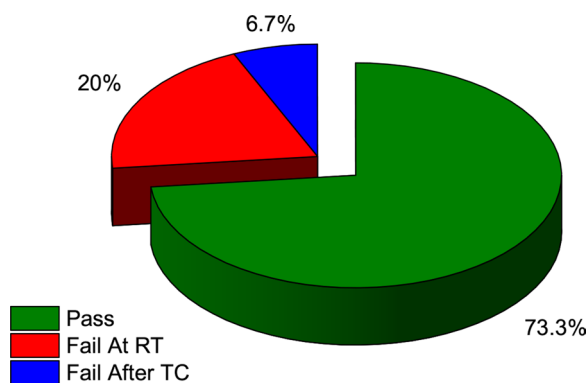

Figure 7: Yield analysis for all N = 30 microstructures fabricated and shear tested at room temperature (RT) and after cryogenic thermal cycling (TC). Of the microstructures tested at room temperature (N = 17), 6 were observed as defective. Of the microstructures tested after cryogenic thermal cycling (N = 13), 2 were observed as defective.

microscopy and optical profilometry. Atomic force microscopy was performed to measure surface roughness and extract elastic modulus from force-distance measurements. Shear tests were performed to identify structural failure modes. A comparison of shear load failure versus height suggested negligible height dependence. Outlier data points from the structure height analysis led to an investigation of fabrication variation (shear load failure versus individual fabricated chips) to identify the source of low shear force failures. Fabrication variation was assumed to be the primary factor of early failure modes. A yield analysis was conducted which demonstrated greater than 70% functional yield achieved across 30 fabricated structures. Structures evaluated in this work give confidence to viability at even lower temperatures since the lowest thermal cycling temperature (77 K) encompassed 74% of the total temperature change (from 300 to 0 K) in which majority of the thermally induced stresses occur. Further refinement of the process can be achieved by increasing the resolution of the TPP print as well as evaluating more complex structures. Additional exploration of various resin materials is of great interest to expand the flexibility of TPP as a technique for cryogenic applications. Processes developed hope to pave the way for additional cryogenic exploration for TPP-fabricated micro/nano structures to further bridge the gap of cryogenic electronics and optical electronics.

Materials and methods

Evaluated microstructures were fabricated by rotational mixing of Sartomer ethoxylated 6 trimethylolpropane triacrylate (SR499), Sartomer tris (2-hydroxyethyl) isocyanurate triacrylate (SR368), and Sigma-Aldrich 2-benzyl-2-(dimethylamino)-4-morpholinobutyrophenone (DBMP) (48.5%, 48.5%, 3.0% by percent mass, respectively). Material combination was selected to prioritize structural stability and minimization of post exposure shrinkage. To facilitate mixing, Sartomer SR368 was heated on a hot plate to 80 °C for 15 min. Once sufficiently heated and melted to a less viscous consistency, SR499 was added by pipette. Mass of each component was directly measured with a microbalance. Mixing of SR368 and SR499 was performed for 20 min, after which DBMP was added to the mixture. Once all components were combined, additional room temperature mixing was performed for 30 min. The resin was then placed in a vial rotator inside a VWR gravity oven set to 40 °C for 12 h to ensure uniform mixing. Without heating the mixture during the long term mixing process, the viscosity of the resin would become too high for sufficient DBMP mixing. A sample of the resin was taken and the representative viscosity of the TPP resin was measured in ambient room temperature with a NDJ-5S viscometer with a #2 rotor standard. Measurements averaged 738 mPa·s across

multiple rotor rotation speeds (6 rpm, 12 rpm, and 30 rpm) at room temperature.

All fabrication was carried out within a yellow room and HEPA-filter environment. TPP was performed using a Spectra-Physics® High-Q2™ fs laser system in conjunction with a Newport Laser µfab™ system. Control of the TPP patterning was facilitated by an x, y, z translation stage, a stationary microscope objective (Olympus PLN20X NA: 0.4, 20x lens), and an electronic shutter. The output of the laser was directed into a neutral density filter followed by the described Newport Laser µfab™ system. The laser power and profile were both captured with a Newport Power Meter Model 843-R with a 919P-030-18 sensor and an Ophir NanoScan 2s beam profiler. The laser environment is shown in Fig. 8.

Si wafers were diced into 20 × 20 mm chips using a dicing saw with a diamond blade. Laser engraving was performed in the center of the Si chips to create alignment marks with a subsequent solvent rinse performed (acetone, methanol, isopropyl alcohol, and DI water) to remove residue prior to TPP fabrication processes. Diced Si samples with etched alignment marks (purchased with 530 nm low-pressure chemical vapor
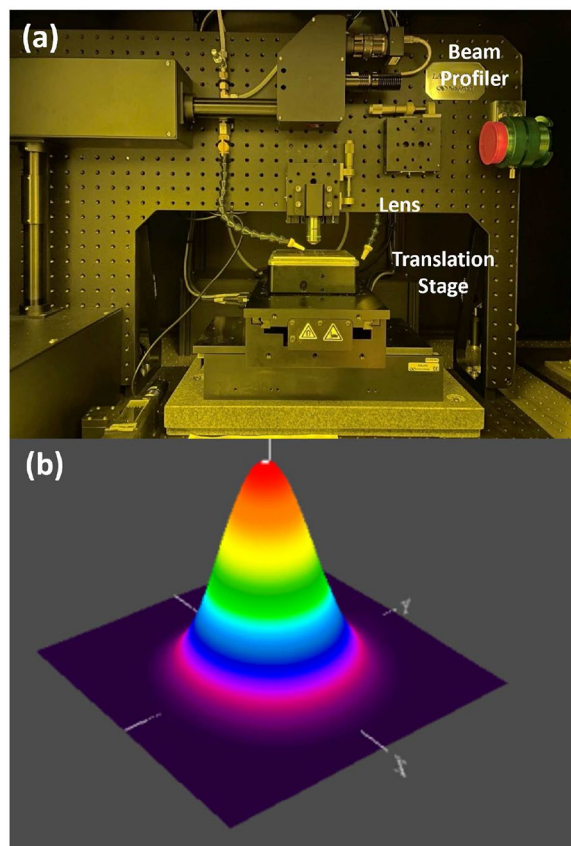

Figure 8: Images detailing the (a) fabrication environment and (b) the beam profile of the laser prior to the objective lens, demonstrating a sufficiently aligned Gaussian beam.

deposition (LPCVD) tetraethylorthosilicate (TEOS) oxide) were prepared with a silanization procedure to improve adhesion of the polymerized acrylic resin to the SiOx. Si samples were dehydration baked at 120 °C for 30 min and were subsequently placed in a covered Petri dish with 2 pipette drops of methacryloxypropytrimethoxysilane (MPTS, commonly used for SU-8 adhesion promotion) for 1 h. Si chips were then placed on a hotplate at 80 °C for 10 min to complete the silanization process. Si chips were mounted with removable adhesives to a polished Si wafer to ensure planarity across the laser exposure target and ~ 60 μm spacers were applied to control the thickness of the resin. Resin was deposited by pipette drops and excess was removed via a squeegee technique with a flat edge disposable applicator.

After the resin was applied to the target chips, the Si chips were then staged in the Newport Laser μfab™ system and focus was adjusted manually by changing the height of the objective from the sample with a dial-based micrometer translation stage. Rectangular designs were designed as a three-dimensional model in Fusion360 to be 400 × 400 μm to be compatible with the shear testing tool dimensions. The design was then imported into the Newport Laser μfab™ system software. Slices of the model were modified such that a single layer would generate the entire volume of the rectangle, however the model can be easily modified for multiple layers for future work. It is important to note that achieving such small features in an imported geometry was non-trivial. Refinement of the mesh during STL file export was necessary to achieve squared corners of the structure. A fill pitch of 1 μm was used to ensure 100% fill in the body of the rectangle. The Spectra-Physics® High-Q2™ was used as the exposure source for these experiments. The source of the laser remained constant throughout the duration of the experiments performed and changes in delivered average power were achieved by controlling an attenuator through the design software. The software controlled the scanning speed, shutter control, and design properties. The pulse duration of the Spectra-Physics® High-Q2™ was manufacturer specified as ~ 200 fs and repetition rate was documented as ~ 63 MHz. The experiments were performed with a scanning speed (the motion of the x and y translation stage during exposure) of 20 μm/sec. No repetitions of the design were used, i.e., points in the design were exposed only once per designed line fill with the only overlaps being of subsequent exposed lines in the line fill sequence.

After exposing the resin with the laser, chips were removed from the system and separated from the polished Si wafer. Post-exposure spray rinsing with methanol, isopropyl alcohol, and DI water was performed to remove excess non-polymerized resin. Spray rinsing was performed to rapidly remove excess resin to minimize swelling that is introduced in typical bathing processes [14]. Each Si chip used in this work was fabricated to house an even number of microstructures. Since shear testing is a destructive means of mechanical evaluation, half of the fabricated structures (in most cases) were available to shear for room temperature (before cryogenic thermal cycling) baseline shear measurements and the remaining half after cryogenic thermal cycling. This allowed for better process analysis and ultimately enabled the observation of process variation dominant defects reducing the possibility of reliability trends with microstructure height and further increasing confidence of the analysis.

Many measurement tools were used to evaluate TPP microstructures in this work. Tapping measurements and force-distance measurements that were performed on a sampling of fabricated structures to extract the elastic modulus in various locations and surface roughness was measured by using an Anton Paar Tosca 400 atomic force microscopy system. Shear tests were completed with a Dage 2400 with a calibrated 500 g tool, positioning the height of the tool consistently 5 μm above the surface of the Si chip or the base of the TPP microstructure. Structure heights were verified by optical profilometry, using a MicroXAM-800 optical profilometer. Scanning electron microscopy images were collected using a Raith eLINE electron beam lithography system. Post room temperature shear testing thermal cycling was performed by way of direct liquid nitrogen (~ 77 K) submersion inside a cryogenic dewar. Samples were submerged for 10 s then removed until temperature warmed via ambient thermalization, completing one thermal cycle. A total of 5 thermal cycles were completed for each chip. It was assumed that capillary forces during cryogenic submersion were negligible and had minimal impact on thermal cycling mechanical degradation due to the large pitch of fabricated microstructures.

Author contributions

SP and JW performed fabrication, testing, and analysis of TPP structures. SB performed SEM operation. AS performed initial shear testing. JS, MA, and MH provided technical guidance.

Data availability

Data and materials supporting the work presented are available upon request.

Code availability

Not applicable.

Declarations

Conflict of interest The authors declare no conflict of interest.

Ethical approval Not applicable.

Consent to participate Not applicable.

Consent to publication Not applicable.

References

1. S. Hasanov, S. Alkunte, M. Rajeshirke et al., Review on additive manufacturing of multi-material parts: progress and challenges. J. Manuf. Mater. Process. **6**(1), 4 (2021). https://doi.org/10.3390/jmmp6010004

2. T.D. Ngo, A. Kashani, G. Imbalzano et al., Additive manufacturing (3D printing): a review of materials, methods, applications and challenges. Compos. B Eng. **143**, 172–196 (2018). https://doi.org/10.1016/j.compositesb.2018.02.012

3. X. Zhou, Y. Hou, J. Lin, A review on the processing accuracy of two-photon polymerization. AIP Adv. **5**(3), 030701 (2015). https://doi.org/10.1063/1.4916886

4. T. Baldacchini, C.N. LaFratta, R.A. Farrer et al., Acrylic-based resin with favorable properties for three-dimensional two-photon polymerization. J. Appl. Phys. **95**(11), 6072–6076 (2004). https://doi.org/10.1063/1.1728296

5. L. Zheng, K. Kurselis, A. El-Tamer et al., Nanofabrication of high-resolution periodic structures with a gap size below 100 nm by two-photon polymerization. Nanoscale Res. Lett. **14**(1), 134 (2019). https://doi.org/10.1186/s11671-019-2955-5

6. K. Cicha, T. Koch, J. Torgersen et al., Young's modulus measurement of two-photon polymerized micro-cantilevers by using nanoindentation equipment. J. Appl. Phys. **112**(9), 094906 (2012). https://doi.org/10.1063/1.4764330

7. O.A. Jimenez Gordillo, S. Chaitanya, Y.C. Chang et al., Plug-and-play fiber to waveguide connector. Opt. Express **27**(15), 20305 (2019). https://doi.org/10.1364/OE.27.020305

8. T. Zandrini, N. Liaros, L.J. Jiang et al., Effect of the resin viscosity on the writing properties of two-photon polymerization. Opt. Mater. Express **9**(6), 2601 (2019). https://doi.org/10.1364/OME.9.002601

9. M. Diamantopoulou, N. Karathanasopoulos, D. Mohr, Stress-strain response of polymers made through two-photon lithography: micro-scale experiments and neural network modeling. Addit. Manuf. **47**(102), 266 (2021). https://doi.org/10.1016/j.addma.2021.102266

10. K. Lee, A. Green, F. Brossard et al., Study of two-photon laser photolithography with SU-8 at cryogenic temperatures, in *2006 Conference on Lasers and Electro-Optics and 2006 Quantum Electronics and Laser Science Conference*. (IEEE, Long Beach, 2006), pp. 1–2. https://doi.org/10.1109/CLEO.2006.4628072

11. K. Ohlinger, Y. Lin, Z. Poole et al., Undistorted 3D microstructures in SU8 formed through two-photon polymerization. AIP Adv. **1**(3), 032163 (2011). https://doi.org/10.1063/1.3646148

12. J. Bauer, A. Guell Izard, Y. Zhang et al., Programmable mechanical properties of two photon polymerized materials: from nanowires to bulk. Adv. Mater. Technol. **4**(9), 1900146 (2019). https://doi.org/10.1002/admt.201900146

13. D. Chen, J. Li, Y. Yuan et al., A review of the polymer for cryogenic application: methods. Mech. Perspect. Polym. **13**(3), 320 (2021). https://doi.org/10.3390/polym13030320

14. T. Baldacchini, M. Zimmerley, C.H. Kuo et al., Characterization of microstructures fabricated by two-photon polymerization using coherent anti-stokes Raman scattering microscopy. J. Phys. Chem. B **113**(38), 12663–12668 (2009). https://doi.org/10.1021/jp9058998

15. R.W. Carpick, N. Agrait, D.F. Ogletree et al., Variation of the interfacial shear strength and adhesion of a nanometer-sized contact. Langmuir **12**(13), 3334–3340 (1996). https://doi.org/10.1021/la9509007

16. B. Yelamanchili, A. Shah, S.E. Peek et al., Face-to-face cable interconnect scheme for thin flexible superconducting stripline cables. IEEE Trans. Appl. Supercond. **32**(4), 1–5 (2022). https://doi.org/10.1109/TASC.2022.3149729